

# A non-orthogonal representation of the chemical space

Tiago F. T. Cerqueira,<sup>1</sup> Silvana Botti,<sup>2</sup> and Miguel A. L. Marques<sup>2, \*</sup>

<sup>1</sup>*CFisUC, Department of Physics, University of Coimbra, Rua Larga, 3004-516 Coimbra, Portugal*

<sup>2</sup>*Research Center Future Energy Materials and Systems of the University Alliance Ruhr and Interdisciplinary Centre for Advanced Materials Simulation, Ruhr University Bochum, Universitätsstraße 150, D-44801 Bochum, Germany*

(Dated: July 1, 2024)

We present a novel approach to generate a fingerprint for crystalline materials that balances efficiency for machine processing and human interpretability, allowing its application in both machine learning inference and understanding of structure-property relationships. Our proposed fingerprint has two components: one representing the crystal structure and the other characterizing the chemical composition. To represent the latter we construct a non-orthogonal space where each axis represents a chemical element and where the angle between the axes quantifies a measure of the similarity between them. The chemical composition is then defined by the point on the unit sphere in this non-orthogonal space. By utilizing dimension reduction techniques we can construct a two-dimensional global map of the space of the thermodynamically stable crystalline compounds. Despite their simplicity, such maps succeed in providing a physical separation of material classes according to basic physical properties. Moreover, this compositional fingerprint can be used as a versatile input for machine learning algorithms, supplanting conventional one-hot representations of the chemical composition.

The last decade has seen a remarkable surge in computational materials science, largely enabled by advances in high-throughput density functional theory and machine learning techniques [1, 2]. These have greatly increased our knowledge and understanding of materials and contributed to the discovery of many compounds with improved properties. Today, inorganic materials databases contain all experimentally known compounds and millions of other hypothetical phases [3–7]. They also combine structural information with data on thermodynamic stability and a wealth of other mechanical, electronic, magnetic, etc. properties.

This explosion of data has brought with it new challenges. One particular challenge we address here is the digital representation of a compound that is both humanly understandable and suitable for materials informatics techniques. In particular, these representations should allow the visualisation of material properties across different compositions and structural types, greatly extending the concept of structure maps [8, 9]. These were originally developed to find correlations between the structural type of a compound and the electron configuration of its constituents, providing insight into the structure of new or hypothetical compounds.

For binary compounds (or multinary compounds where only two chemical species vary) it is often easy to produce two-dimensional maps where the  $x$ - and  $y$ - axes run through the periodic table (see, e.g., Refs. [10–13]). The order of the elements may simply reflect the atomic number, or some other ordering such as electronegativity or the Pettifor scale and its generalizations [9, 12, 14–16]. The latter is particularly interesting because it reflects the similarity between chemical elements and gives the systematic variation of the property over the binary

composition range. Unfortunately, for ternary or multinary compounds, or when the dataset contains materials with different crystal structures, the production of such material maps is much more complicated.

In fact, it is very difficult to represent material space in a way that allows visualisation — and interpretation — of how material properties vary across a given set of compounds. A common solution is to use machine learning embeddings, which are readily available from most neural network architectures. For example, in crystal graph networks [17] we can use the feature vector obtained after pooling the graph. These can then be used in conjunction with dimension reduction techniques [18, 19] to produce two-dimensional (or higher dimensional) maps that can be used to visualise material properties over material space [20, 21]. Unfortunately, trained embeddings already contain information about the target property (or properties), which often complicates the interpretation of structure-property relationships.

To solve this problem, we need a representation of a material in a vector space (also sometimes called fingerprint, descriptor, or embedding), based only on its chemical composition and crystal structure, such that the distances between points (i.e. compounds) reflect the degree of similarity between these compounds. Here we propose such a fingerprint and show how it can be used to visualise property maps over material space.

We divide the fingerprint into two parts. The first should be a representation of the crystal structure of the materials. Fortunately, there are already several structural fingerprints available in the literature. We will use the one available in PYMATGEN, which measures the similarity between two structures based on local coordination information from all sites in the crystal structures [22]. This representation meets our twin requirements of being machine-friendly and based on a solid human understanding of the underlying physics.

\* miguel.marques@rub.de

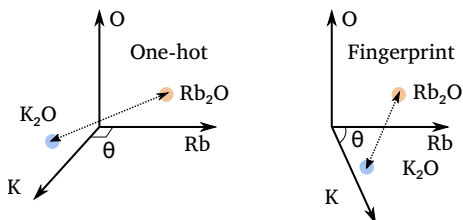


FIG. 1. Schema depicting the distance between  $\text{K}_2\text{O}$  (blue dot) and  $\text{Rb}_2\text{O}$  (brown dot) in a one-hot representation and in our fingerprint space.

For the description of the chemical composition a common solution is to use a one-hot vector, where each element represents a chemical element, a vector constructed from the properties of the elements [17, 23], or machine-learned representations [24]. Unsurprisingly, the latter are more efficient for machine learning [25] but are opaque and not interpretable by humans. Here we propose a scheme that retains the usefulness of these approaches and, at the same time, is simple and fully human understandable. We start with a measure of the similarity between chemical elements, such as the Euclidean distance between the initial (untrained) embeddings of the chemical elements, as provided by MATMINER for example. Here we will use the similarity scale proposed by some of us in Ref. [26], which was constructed by simple statistical arguments using the experimentally known inorganic compounds present in ICSD [27].

We start with the raw data from Ref. [26], which is in the form of a (symmetric) matrix whose dimensions are given by the total number of chemical elements. The off-diagonal elements of the matrix count, for each pair of chemical elements (A, B), the number of compounds in ICSD that have the same crystal structure but where A is replaced by B. In the diagonal elements of the matrix we insert the total number of compounds in ICSD that contain the given element (which can be interpreted as self-substitutions). We then set the upper triangle of the matrix to zero (to remove the duplicated information) and normalise the rows to one so that the entries can be interpreted as a measure of similarity.

Mainly due to the incomplete information present in the ICSD, the off-diagonal components are underestimated with respect to the diagonal. To compensate for this, we decided to modify the matrix elements by raising them by a power of  $\alpha = 1/2$ , followed by a renormalisation of the lines. The resulting matrix is called  $\mathcal{S}$ . We then interpret each row  $\mathcal{S}_i$  of the lower triangular matrix  $\mathcal{S}$  as the Cartesian coordinates of the unit vector representing the corresponding chemical element. This means that the off-diagonal components are the cosines of the angles formed by the unit vectors defining a non-orthogonal compositional space. Completely dissimilar chemical elements are represented by orthogonal unit vectors, with the angle decreasing as the similarity increases. Note that while the non-orthogonal space still has a di-

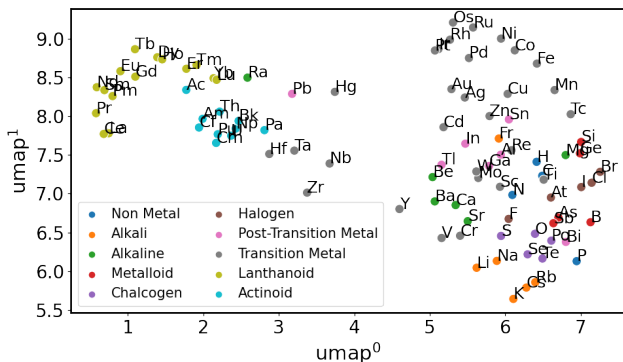


FIG. 2. Two-dimensional map obtained by reducing the dimensions of the compositional fingerprints of the chemical elements. The axes indicate the two dimensions returned by UMAP. The points are coloured according to the group of the periodic table to which the elements belong.

mension equal to the number of chemical elements (since all elements are dissimilar to some extent), the hypercube generated by the non-orthogonal vectors has a smaller volume than in Cartesian space.

To obtain the fingerprint of a given composition, we first create a one-hot composition vector  $c$ , whose dimension is given by the total number of chemical elements and is then normalised so that it lies in the unit hypersphere in the non-orthogonal space. The fingerprint  $f$  is then given in Cartesian coordinates by  $f = c \times \mathcal{S}$ . The distances between the chemical compositions, which measure their dissimilarity, are then simply calculated as the Cartesian distance between the fingerprints. An example is shown in fig. 1 where we plot  $\text{K}_2\text{O}$  (blue dot) and  $\text{Rb}_2\text{O}$  (brown dot) in a standard one-hot representation and in our fingerprint space. The angle between K and Rb in our space is about  $66^\circ$  (while K and Rb remain orthogonal to O due to their dissimilarity), making the distance between the two compounds closer than in a one-hot Euclidean representation.

To illustrate the results of this construction, we calculated the compositional fingerprints of the chemical elements, given by the lines of the matrix  $\mathcal{S}$ . To represent this data as a map, we performed a dimension reduction using the Uniform Manifold Approximation and Projection (UMAP) [19]. The resulting two-dimensional map, which can be thought of as a data-mined and machine-learned periodic table, is shown in fig. 2. We have removed noble gases (which rarely form compounds) and actinides for which there are no compounds in ICSD, and have coloured the points according to the group of the periodic table.

From the construction, we expect similar chemical elements to be close together in the map, although the reduction to only two dimensions may distort the distances in the  $> 80$ -dimensional composition space. We also note that the actual shape of the map depends on the parameters of UMAP (such as the number of neigh-

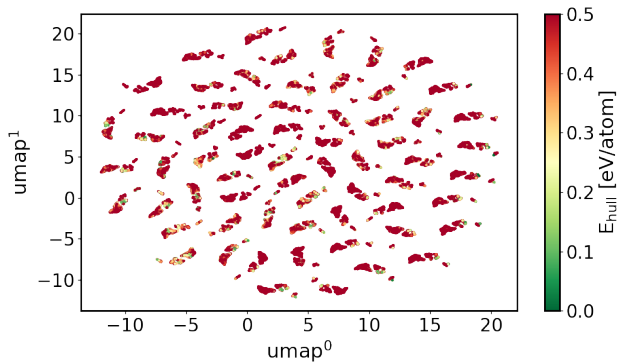


FIG. 3. Composition map of cubic  $ABX_3$  perovskites projected into two dimensions with UMAP (considering only the composition). For the plot we chose the structure  $ABX_3$  or  $BAX_3$  with the lowest energy. Points are coloured according to their distance to the convex hull of the corresponding material, capped to 0.5 eV/atom.

hours or the minimum distance used by UMAP to decide how closely points are packed together), but the relative distribution of chemical elements is quite robust.

Indeed, looking at fig. 2 we see that related elements tend to be packed together, with those belonging to the same group of the periodic table usually found in tightly packed groups. On the left are the lanthanides and actinides, on the top right are most of the transition metals, and on the bottom right are most of the other elements (non-metals, alkalis, alkaline-earths, etc). Interestingly, Zr, Nb, Hf, Ta, Pb and Hg are between the two groups.

As another example, we show in fig. 3 a similar analysis performed on the dataset of perovskites with composition  $ABX_3$  from Ref. 28. We note that the compounds in this dataset all share the same structure, namely the cubic  $Pm\bar{3}m$  (space group #221) with five atoms in the unit cell and undistorted octahedra. The figure provides therefore only a map of the composition. As both compounds  $ABX_3$  and  $BAX_3$  have the same chemical composition, and therefore the same compositional fingerprint, we plot only the phase with the lowest energy. The points are coloured according to their distance from the convex hull of thermodynamic stability. Since the chemical composition is dominated by the atom X, the map is naturally divided into clusters, one for each X. The distribution of the clusters is then largely determined by the similarity between the X atoms. Within each cluster, there is a fine structure that reflects the similarity between the A and B atoms.

It is clear from the figure that most cubic perovskites are highly unstable, but some islands of higher stability can be seen. The well-known oxide perovskites  $ABO_3$  are centred at the coordinates  $(-3, 8)$ , with hydride perovskites  $ABH_3$  just below. However, most stable (or near stable) compounds are inverted perovskites with an H, C, N, O, etc. in the Wyckoff 1b position. These can be seen as green dots, usually at the boundaries of the clus-

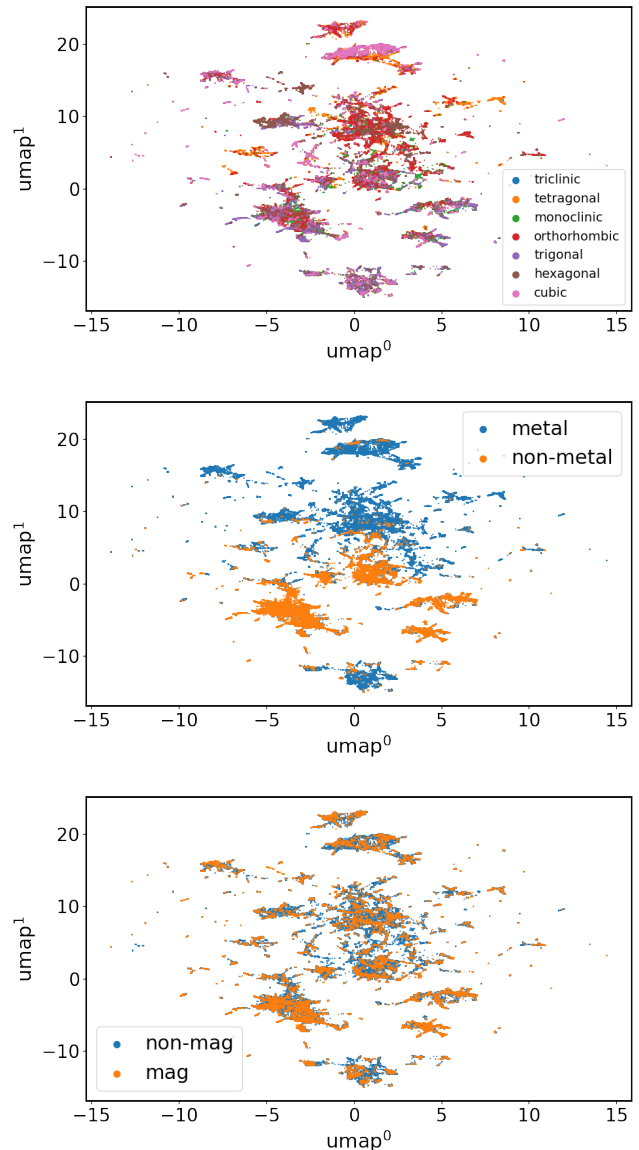


FIG. 4. Materials on the convex hull of Alexandria, projected into two dimensions using UMAP (taking into account both structure and chemical composition). We distinguish by crystal system (top), between metallic and semiconducting materials (middle), and between magnetic and non-magnetic materials (bottom).

ters. By far the more stable systems are the inverted perovskites of the type  $ABCa_3$  at  $(-6, -7)$ ,  $ABSr_3$  at  $(2, -2)$ ,  $ABSc_3$  at  $(-2, -2)$ , etc.

To compute structure maps of compounds with arbitrary structures, we can concatenate the structure and composition fingerprints. These can be combined with different weights, depending on whether you want to give more weight to the composition or the structure. For simplicity, we have chosen equal weights for both fingerprints in the following. As an example of this procedure, we plot in fig. 4 the map of all thermodynamically

stable materials, i.e. compounds that lie on the convex hull of thermodynamic stability, found in the alexandria database. This corresponds to over 115 thousand compounds with a wide variety of chemical compositions and structural types. To reduce the number of dimensions to two, we again use UMAP. We also color the points according to the crystal system, the existence of an electronic band gap (metal / non-metal, or the existence of finite magnetic moments (magnetic / non-magnetic)).

As a full discussion of the materials on the convex hull and their properties goes well beyond the scope of this work, we limit ourselves to a few general observations. UMAP divides the vast majority of the compounds into large ‘‘continents’’, with a few materials scattered in smaller islands. While the actual two-dimensional map is highly dependent on the parameters of UMAP, it is reasonable to interpret these smaller islands as more structurally and compositionally exotic compounds with few related materials on the convex hull. It is interesting to see that, despite the extremely large diversity of the data set, the map provides a reasonable structural separation of compounds - indeed, some of the continents and islands are predominantly dominated by compounds of a particular crystal system. Furthermore, other islands correctly identify similar structural motifs, such as the hexagonal and trigonal symmetry adopted by many layered materials, or the cubic, tetragonal, orthorhombic sequence often obtained for many compounds as symmetry decreases with, for example, decreasing temperature. The middle panel of fig. 4 is interesting as it shows that UMAP combined with our fingerprint provides an excellent separation between metals and semiconducting or insulating compounds. Indeed we observe that the latter are concentrated in the lower part of the figure (roughly between  $umap_1$  between -10 and 5), with metal concentrated on the southernmost island and most of the northern hemisphere. Interestingly, such a good separation is not visible in the bottom panel, which represents magnetic and non-magnetic compounds. This suggests that, unfortunately, this distinction will be much more difficult to predict with machine learning approaches than the previous properties.

An interesting question concerns the actual number of dimensions needed in practice to represent all the materials on the hull. Our fingerprint vector contains  $61 \times 4 = 244$  elements to represent the structure, to which we add one extra dimension per chemical element. The question is how many of these  $> 300$  dimensions are really needed. We can get this information by performing a principal component analysis of the data. We find that only 9 components are sufficient to represent 50% of the variance in composition, while 7 are required to represent 50% of the variance in composition and structure. If we ask for 95%, we need 54 components for composition and 76 for composition and structure. This is much smaller than the original number of components, meaning that it may be possible to compress the information into a smaller feature vector that is more suitable for efficient

machine learning of materials data.

dataset	HotCrab	CrabNet	this work
aflow bulk modulus	9.49	8.87	8.92
aflow Debye temp.	36.6	33.5	34.5
aflow shear modulus	9.94	9.40	9.54
aflow thermal cond.	2.53	2.44	2.45
aflow thermal expansion	4.75e-6	4.06e-6	4.28e-6
aflow $E_{\text{gap}}$	0.335	0.322	0.318
aflow energy/atom	0.116	0.107	0.108
CritExam Ed	0.0669	0.0631	0.0644
CritExam Ef	0.0747	0.0758	0.0782
MP bulk modulus	12.4	11.8	11.8
MP Ehull	0.0982	0.0932	0.0941
MP elastic anisotropy	8.16	8.15	8.32
MP $\mu_b$	2.32	2.22	2.34
MP shear modulus	13.4	13.0	12.6
OQMD abndgap	0.0576	0.0587	0.0558
OQMD energy/atom	0.0514	0.0518	0.0522
OQMD form. Enthalpy	0.0441	0.0438	0.0406
OQMD volume/atom	0.315	0.331	0.319

TABLE I. Mean absolute error for a series of datasets using crabnet with one-hot representation of the chemical composition, mat2vec [24], and the fingerprint presented in this work. For a description of the datasets see Ref. 25.

Finally, we used our fingerprint to represent compounds in compositional neural network models. Specifically, we used the compositionally-restricted attention-based network (CrabNet [25]) for predicting materials properties using the mat2vec [24] representation. These information-dense word embeddings were constructed by unsupervised learning from a huge body of scientific literature. We also compare them to the one-hot encoding of the chemical composition (HotCrab). We present results for 20 benchmarks covering a wide range of material properties and dataset sizes. We see from table I that our constructed representation replaces HotCrab and is on a par with CrabNet, while retaining simplicity and interpretability. Of course, our fingerprint can only be used as a node embedding in graph neural networks (or in other architectures), but this is beyond the scope of this work.

In conclusion, we propose a fingerprint function that provides a simple and interpretable representation of the chemical composition of a compound. This is designed so that the distance between fingerprints of compounds that are chemically similar - and therefore likely to have similar materials properties - is smaller than for unrelated materials. We show how this fingerprint can be used to create structure maps, or more generally property maps, spanning entire families of materials, or even the entire material space. Such maps can be used to visualise and interpret how materials properties change across chemical space. Finally, we show that our human-generated fingerprint can compete with machine-learned opaque representations when it is used as input feature to machine learning models. There are still some shortcomings in our approach, such as the lack of information for rare gases or some actinides, but we believe that our

representation of the chemical space can already be an important tool both for accurate machine prediction of material properties and for human interpretation of high-throughput investigations.

## I. DATA AND CODE AVAILABILITY

The data used in this work, along with the accompanying example notebook, is available on GitHub at <https://github.com/hyllios/utis/tree/main/similarity>

## II. ACKNOWLEDGEMENTS

T.F.T.C acknowledges financial support from FCT - Fundação para a Ciência e Tecnologia, I.P. through the project CEECINST/00152/2018/CP1570/CT0006 with DOI identifier 10.54499/CEECINST/00152/2018/CP1570/CT0006.

## III. COMPETING INTERESTS

The authors declare that they have no competing interests.

- 
- [1] J. Schmidt, M. R. G. Marques, S. Botti, and M. A. L. Marques, Recent advances and applications of machine learning in solid-state materials science, *npj Comput. Mater.* **5**, 10.1038/s41524-019-0221-0 (2019).
- [2] H. J. Kulik, T. Hammerschmidt, J. Schmidt, S. Botti, M. A. L. Marques, M. Boley, M. Scheffler, M. Todorović, P. Rinke, C. Oses, A. Smolyanyuk, S. Curtarolo, A. Tkatchenko, A. P. Bartók, S. Manzhos, M. Ihara, T. Carrington, J. Behler, O. Isayev, M. Veit, A. Grisafi, J. Nigam, M. Ceriotti, K. T. Schütt, J. Westermayr, M. Gastegger, R. J. Maurer, B. Kalita, K. Burke, R. Nagai, R. Akashi, O. Sugino, J. Hermann, F. Noé, S. Pilati, C. Draxl, M. Kuban, S. Rigamonti, M. Scheidgen, M. Esters, D. Hicks, C. Toher, P. V. Balachandran, I. Tamblin, S. Whitelam, C. Bellinger, and L. M. Ghiringhelli, Roadmap on machine learning in electronic structure, *Electron. Struct.* **4**, 023004 (2022).
- [3] J. Schmidt, N. Hoffmann, H.-C. Wang, P. Borlido, P. J. M. A. Carriço, T. F. T. Cerqueira, S. Botti, and M. A. L. Marques, Machine-learning-assisted determination of the global zero-temperature phase diagram of materials, *Adv. Mater.* **35**, 2210788 (2023).
- [4] A. Jain, S. P. Ong, G. Hautier, W. Chen, W. D. Richards, S. Dacek, S. Cholia, D. Gunter, D. Skinner, G. Ceder, and K. A. Persson, Commentary: The materials project: A materials genome approach to accelerating materials innovation, *APL Mater.* **1**, 011002 (2013).
- [5] S. Curtarolo, W. Setyawan, S. Wang, J. Xue, K. Yang, R. H. Taylor, L. J. Nelson, G. L. Hart, S. Sanvito, M. Buongiorno-Nardelli, N. Mingo, and O. Levy, AFLOWLIB.ORG: A distributed materials properties repository from high-throughput ab initio calculations, *Comput. Mater. Sci.* **58**, 227 (2012).
- [6] J. E. Saal, S. Kirklin, M. Aykol, B. Meredig, and C. Wolverton, Materials design and discovery with high-throughput density functional theory: The open quantum materials database (oqmd), *JOM* **65**, 1501–1509 (2013).
- [7] K. Choudhary, K. F. Garrity, A. C. E. Reid, B. DeCost, A. J. Biacchi, A. R. Hight Walker, Z. Trautt, J. Hatrick-Simpers, A. G. Kusne, A. Centrone, A. Davydov, J. Jiang, R. Pachter, G. Cheon, E. Reed, A. Agrawal, X. Qian, V. Sharma, H. Zhuang, S. V. Kalinin, B. G. Sumpter, G. Pilania, P. Acar, S. Mandal, K. Haule, D. Vanderbilt, K. Rabe, and F. Tavazza, The joint automated repository for various integrated simulations (jarvis) for data-driven materials design, *npj Comput. Mater.* **6**, 10.1038/s41524-020-00440-1 (2020).
- [8] P. Villars, K. Mathis, F. Hulliger, F. De Boer, and D. Pettifor, *Environment classification and structural stability maps*, Vol. 1 (Elsevier Science Publishing BV, 1989).
- [9] D. G. Pettifor, A chemical scale for crystal-structure maps, *Solid State Commun.* **51**, 31 (1984).
- [10] A. Silva, J. Cao, T. Polcar, and D. Kramer, Pettifor maps of complex ternary two-dimensional transition metal sulfides, *npj Comput. Mater.* **8**, 10.1038/s41524-022-00868-7 (2022).
- [11] M. Fukuda, J. Zhang, Y.-T. Lee, and T. Ozaki, A structure map for ab2 type 2d materials using high-throughput dft calculations, *Mater. Adv.* **2**, 4392–4413 (2021).
- [12] A. Silva, J. Cao, T. Polcar, and D. Kramer, Design guidelines for two-dimensional transition metal dichalcogenide alloys, *Chem. Mater.* **34**, 10279–10290 (2022).
- [13] W. Chen, A. Hilhorst, G. Bokas, S. Gorsse, P. J. Jacques, and G. Hautier, A map of single-phase high-entropy alloys, *Nat. Commun* **14**, 10.1038/s41467-023-38423-7 (2023).
- [14] D. Pettifor, The structures of binary compounds. i. phenomenological structure maps, *J. Phys. C: Solid State Phys.* **19**, 285 (1986).
- [15] H. Glawe, A. Sanna, E. Gross, and M. A. Marques, The optimal one dimensional periodic table: a modified pettifor chemical scale from data mining, *New J. Phys.* **18**, 093011 (2016).
- [16] Z. Allahyari and A. R. Oganov, Nonempirical definition of the mendelev numbers: Organizing the chemical space, *J. Phys. Chem. C* **124**, 23867–23878 (2020).
- [17] T. Xie and J. C. Grossman, Crystal graph convolutional neural networks for an accurate and interpretable prediction of material properties, *Phys. Rev. Lett.* **120**, 10.1103/physrevlett.120.145301 (2018).
- [18] K. Pearson, Liii. on lines and planes of closest fit to systems of points in space, *London Edinburgh Philos. Mag. & J. Sci.* **2**, 559–572 (1901).
- [19] L. McInnes, J. Healy, and J. Melville, Umap: Uniform manifold approximation and projection for dimension reduction (2018).
- [20] T. Xie and J. C. Grossman, Hierarchical visualization of materials space with graph convolutional neural net-

- works, *J. Chem. Phys.* **149**, 10.1063/1.5047803 (2018).
- [21] A. Y.-T. Wang, M. S. Mahmoud, M. Czasny, and A. Gurlo, Crabnet for explainable deep learning in materials science: Bridging the gap between academia and industry, *Integr. Mater. Manuf. Innov.* **11**, 41–56 (2022).
- [22] N. E. Zimmermann, M. K. Horton, A. Jain, and M. Haranczyk, Assessing local structure motifs using order parameters for motif recognition, interstitial identification, and diffusion path characterization, *Front. Mater.* **4**, 34 (2017).
- [23] L. Ward, A. Dunn, A. Faghaninia, N. E. Zimmermann, S. Bajaj, Q. Wang, J. Montoya, J. Chen, K. Bystrom, M. Dylla, K. Chard, M. Asta, K. A. Persson, G. J. Snyder, I. Foster, and A. Jain, Matminer: An open source toolkit for materials data mining, *Comput. Mater. Sci.* **152**, 60–69 (2018).
- [24] V. Tshitoyan, J. Dagdelen, L. Weston, A. Dunn, Z. Rong, O. Kononova, K. A. Persson, G. Ceder, and A. Jain, Unsupervised word embeddings capture latent knowledge from materials science literature, *Nature* **571**, 95–98 (2019).
- [25] A. Y.-T. Wang, S. K. Kauwe, R. J. Murdock, and T. D. Sparks, Compositionally restricted attention-based network for materials property predictions, *npj Comput. Mater.* **7**, 10.1038/s41524-021-00545-1 (2021).
- [26] H.-C. Wang, S. Botti, and M. A. Marques, Predicting stable crystalline compounds using chemical similarity, *npj Comput. Mater.* **7**, 12 (2021).
- [27] D. Zagorac, H. Müller, S. Ruehl, J. Zagorac, and S. Rehme, Recent developments in the inorganic crystal structure database: theoretical crystal structure data and related features, *J. Appl. Crystallogr.* **52**, 918–925 (2019).
- [28] J. Schmidt, J. Shi, P. Borlido, L. Chen, S. Botti, and M. A. L. Marques, Predicting the thermodynamic stability of solids combining density functional theory and machine learning, *Chem. Mater.* **29**, 5090–5103 (2017).